

Open-Set Deepfake Detection: A Parameter-Efficient Adaptation Method with Forgery Style Mixture

Chenqi Kong, *Member, IEEE*, Anwei Luo, Peijun Bao, Haoliang Li, *Member, IEEE*, Renjie Wan, *Member, IEEE*, Zengwei Zheng, Anderson Rocha, *Fellow, IEEE*, and Alex C. Kot *Life Fellow, IEEE*

Abstract—Open-set face forgery detection poses significant security threats and presents substantial challenges for existing detection models. These detectors primarily have two limitations: they cannot generalize across unknown forgery domains and inefficiently adapt to new data. To address these issues, we introduce an approach that is both general and parameter-efficient for face forgery detection. It builds on the assumption that different forgery source domains exhibit distinct style statistics. Previous methods typically require fully fine-tuning pre-trained networks, consuming substantial time and computational resources. In turn, we design a forgery-style mixture formulation that augments the diversity of forgery source domains, enhancing the model’s generalizability across unseen domains. Drawing on recent advancements in vision transformers (ViT) for face forgery detection, we develop a parameter-efficient ViT-based detection model that includes lightweight forgery feature extraction modules and enables the model to extract global and local forgery clues simultaneously. We only optimize the inserted lightweight modules during training, maintaining the original ViT structure with its pre-trained ImageNet weights. This training strategy effectively preserves the informative pre-trained knowledge while flexibly adapting the model to the task of Deepfake detection. Extensive experimental results demonstrate that the designed model achieves state-of-the-art generalizability with significantly reduced trainable parameters, representing an important step toward open-set Deepfake detection in the wild. The code is available at <https://github.com/ChenqiKONG/OSDFD>.

Index Terms—Deepfakes, face forgery detection, open-set, style mixture, generalization, robustness, parameter-efficient learning.

I. INTRODUCTION

THE rapid advancement of Artificial Intelligence Generated Content (AIGC) has led to significant progress in face forgery techniques, producing increasingly sophisticated fake faces that are indistinguishable from the human eye. Such advancements have fueled the proliferation of multimedia content on social media, posing high risks of disinformation, misinformation, and identity theft [1]. The recent emergence of

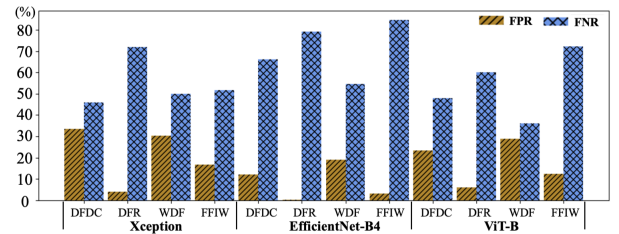


Fig. 1. False Positive Rates (FPR) and False Negative Rates (FNR) of Xception, EfficientNet-B4, and ViT-B on four unforeseen Deepfake datasets: DFDC, DFR, WDF, and FFIW.

diffusion and other advanced large vision-language models has exacerbated these challenges [2]. Consequently, developing effective detection methods to combat digital face forgery attacks has become critically important [3].

Face forgery detection has long posed a challenging yet crucial problem. Early methodologies proposed extracting hand-crafted features such as LBP maps [4], color components [5], and DCT maps [6] as informative indicators for Deepfake detection. Subsequent works focused on capturing anomalies like eye-blinking [7], head pose artifacts [8], and face-warping features [9]. Many methods aimed to improve detection accuracy by developing learning-based models using generic architectures such as Xception Net [10], Efficient Net [11], and Capsule Net [12]. Later approaches, including Face X-ray [13], SBI [14], DCL [15], and RECCE [15] sought to capture common forgery features to enhance model generalizability. With the advent of ViT [16], numerous ViT-based detectors [17]–[20] have been developed. These approaches exploit global receptive fields and exhibit superior detection performance.

However, previous face forgery detection methods still face two major challenges in real-world applications: (1) Existing methods struggle to generalize in uncontrolled environments. These models may encounter unforeseen forgery domains in the wild, which can lead to significant performance degradation; (2) In practical scenarios, detection models often require fine-tuning newly acquired data to adapt to new domains. However, adapting pre-trained detection models to new data is computationally costly and impedes deployment in real-world settings, especially on mobile devices with limited computing resources.

To address these two challenges, this paper introduces a generalized and parameter-efficient approach for **Open-Set DeepFake Detection (OSDFD)**. Different forgery-style statistics may exhibit unique properties critical for face forgery

C. Kong, P. Bao, and A. C. Kot are with the Rapid-Rich Object Search (ROSE) Lab, School of Electrical and Electronic Engineering, Nanyang Technological University, Singapore, 639798. (email: chenqi.kong@ntu.edu.sg, peijun001@e.ntu.edu.sg, eackot@ntu.edu.sg.)

A. Luo is with the School of Computer Science and Engineering, Sun Yat-sen University, Guangzhou, China. (email: luowan@mail2.sysu.edu.cn).

R. Wan is with the Department of Computer Science, Hong Kong Baptist University, Hong Kong SAR. (email: renjiewan@hkbu.edu.hk).

H. Li is with the Department of Electrical Engineering, City University of Hong Kong, Hong Kong SAR. (email: haoliang.li@cityu.edu.hk).

Z. Zheng is with the Department of Computer Science and Computing, Zhejiang University City College, Zhejiang, China. (email: zhengzw@zucc.edu.cn).

A. Rocha is with the Artificial Intelligence Lab. (Recod. ai) at the University of Campinas, Campinas 13084-851, Brazil (e-mail: arrocha@unicamp.br), URL: <http://recod.ai>

detection. Fig. 1 shows that existing forgery detectors have a significantly higher false negative rate (FNR) than the false positive rate (FPR) in unforeseen forgery domains, indicating a tendency to misclassify fake faces as real when encountering new domains in uncontrolled environments. Grounded in this observation, we propose a forgery style mixture module that enhances the diversity of source forgery domains by randomly mixing the feature statistics of different forgery styles, thereby effectively improving the model’s generalizability.

Furthermore, most prior art utilizes generic CNNs and ViTs as backbones and fully fine-tune the networks from ImageNet weights. However, fully fine-tuning a network is costly, hindering its real-world applications. To mitigate this issue, we integrate lightweight Adapter and LoRA layers into the ViT backbone. During training, we freeze plain ViT backbones with ImageNet weights and solely update the lightweight Adapter and LoRA layers. These designed modules capture local and global forgery artifacts using slim components. Additionally, these modules preserve substantial ImageNet knowledge and enable flexible model adaptation for face forgery detection. Fig. 2 illustrates the average cross-dataset AUC performance across six unforeseen Deepfake datasets versus the number of activated parameters. This demonstrates that our method achieves superior generalizability with the fewest activated parameters.

This work extends upon our previous conference work [21]. The main distinctions between this work and [21] are summarized as follows: (1) We introduce the Central Difference Convolution (CDC) adapter to incorporate local forgery priors into the expressive ViT model, thereby enhancing the model’s detection performance, (2) We propose a forgery style mixture module that combines source forgery domains to improve the model’s generalizability across unforeseen forgery domains; (3) We further reduce the dimension of LoRA layers, enabling more parameter-efficient face forgery detection; (4) We conduct extensive additional experiments compared with more SOTA methods, including cross-dataset evaluations, robustness experiments, visualization results, and ablation studies.

In summary, the main contributions of this work are as follows:

- We design a forgery-style mixture module to enhance the diversity of source domains. The model’s generalizability is effectively improved by randomly mixing forgery styles.
- We introduce a CDC adapter and a LoRA module into pre-trained plain ViT models. This design successfully captures forgery-related features and enables parameter-efficient face forgery detection.
- We carry out extensive experiments and demonstrate that our model achieves state-of-the-art generalizability and robustness with only 1.34M activated parameters.

We arranged the remaining of this paper into four more sections, Sec. II comprehensively reviews previous literature on face forgery detection and parameter-efficient fine-tuning. Sec. III details the proposed detection framework. Sec. IV presents extensive experimental results under various settings—finally, Sec. V concludes the paper and discusses possible future research directions.

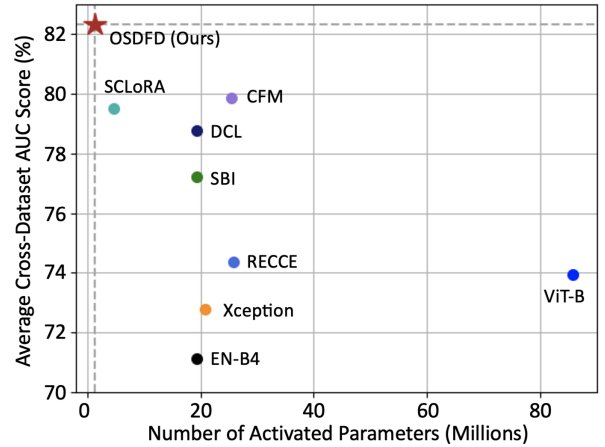


Fig. 2. Average cross-dataset AUC score across six unseen datasets vs. the number of activated parameters. Our OSDFD method achieves the best generalizability with the fewest trainable parameters.

II. RELATED WORK

A. Face forgery detection

Early face forgery detection methods initially focused on extracting hand-crafted features, such as eye-blinking frequency [7], head pose inconsistency [8], face warping artifacts [9], and rPPG features [22]. With the rise of deep learning and artificial intelligence, numerous learning-based methods emerged to improve detection accuracy. Some generic CNNs, such as the Xception network [6], [10], [23], [24], EfficientNet-b4 [11], [25], and Capsule network [12], have been utilized for face forgery detection, showing promising results. However, these methods often need to be more balanced in training data, leading to poor generalization capabilities. In response, some approaches have focused on extracting common forgery features. For example, Face X-ray [13] and SBI [14] aimed to extract common face blending features, enhancing model generalizability. F³Net and Luo et al. [24] mined frequency artifacts, while DCL [15] and CFM [25] employed contrastive learning schemes for more generalized Deepfake detection. With the rapid advancements in vision transformers (ViT), several ViT-based approaches [17]–[19], [21], [26]–[28] have been developed, showing superior detection performance. ICT [17] introduced the Identity Consistency Transformer to capture identity inconsistency within fake faces, while F²Trans designed the High-Frequency Fine-Grained Transformer, achieving more generalized and robust forgery detection. However, the scalability of ViT-based methods is largely constrained by the quadratic complexity of attention computation, limiting their deployment, particularly on mobile devices with limited computing resources. In response, this paper introduces a parameter-efficient fine-tuning (PEFT) strategy for face forgery detection to address this issue. Furthermore, we combine different forgery styles to augment the forgery source domains, enhancing the model’s generalization capability.

B. Parameter-efficient fine-tuning (PEFT)

The attention mechanism has demonstrated significant success across various computer vision tasks. However, the self-

attention in ViT scales quadratically concerning the input patch number, leading to substantial computational demands during training. Several methods have been proposed to address this issue, including parameter-efficient fine-tuning (PEFT). PEFT selectively updates a small portion of the model parameters, facilitating model adaptation to downstream tasks. Adapters [29], [30] are typically inserted between feedforward and normalization layers of transformers, comprising a down-sample and up-sample layer. For example, Low-Rank Adaptation (LoRA) [31] decomposes a matrix into two trainable low-rank matrices, significantly reducing the number of parameters compared to the original matrix. Visual Prompt Tuning (VPT) [32] introduces a small number of trainable parameters in the input space, treating additional tokens as learnable pixels. Convpass [33] aims to inject local priors into expressive ViT models by integrating convolutional operations, enhancing performance across various computer vision tasks. Neural Prompt Search (NOAH) [34] further advances by incorporating Adapter, LoRA, and VPT into vision transformers and optimizing their design through a neural architecture search algorithm. Despite these advancements, the development of PEFT methods for face forgery detection has been largely understudied, yet it is crucial in practical scenarios. In this paper, we integrate lightweight Adapter and LoRA modules into the plain ViT backbone, optimizing only these modules while keeping the ViT backbone fixed with ImageNet weights during training. The designed modules effectively capture global and local face forgery features more efficiently, without the danger of catastrophic forgetting typical of fully finetuning models [35].

III. PROPOSED METHOD

A. Overall framework

Fig. 3 illustrates the overview of the proposed face forgery detection method. The designed framework relies upon ViT, which is pre-trained on ImageNet as the backbone. As Fig. 3 (a) depicts, the features extracted by the transformer blocks are fed forward to the Forgery Style Mixture module. This module exclusively mixes the statistics of forgery styles, augmenting the forgery source domains during training. The processed features are delivered to the MLP head for the final decision-making. Fig. 3 (b) illustrates the details of transformer blocks. We insert the trainable Adapter and LoRA layers into the ViT block. The ViT backbone is fixed with pre-trained ImageNet weights. Fig. 3 (c) and Fig. 3 (d) detail the Adapter and LoRA layers. In Fig. 3 (c), the input hidden state h^{in} is followed by three trainable convolutional layers. Moreover, h^{in} is simultaneously multiplied with the ImageNet pretrained weight. The output hidden state h^{out} is the element summation of the two features. In turn, the LoRA layer dedicated in Fig. 3 (d) introduces two trainable low-rank matrices $W^{down} \in \mathbb{R}^{d \times r}$ and $W^{up} \in \mathbb{R}^{r \times d}$, where $r \ll d$. Moreover, h^{out} is obtained by conducting an element-wise summation of the two outputs.

B. Forgery-aware PEFT

Our proposed method aims to capture critical forgery clues using lightweight modules to facilitate face forgery detection

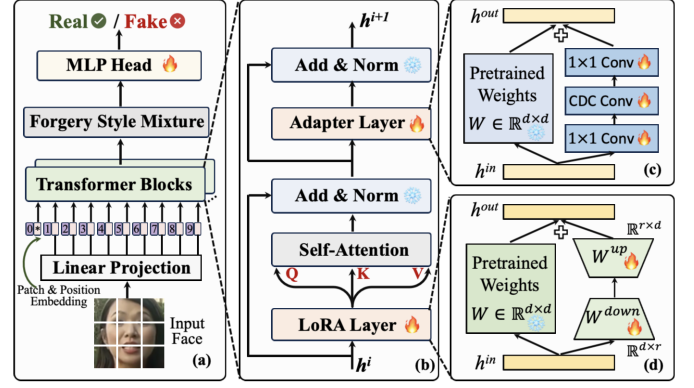


Fig. 3. Overview of the designed face forgery detection framework. (a) Overall model structure; (b) Structure of the designed transformer block; (c) Details of the designed adapter layer; (d) Details of the designed LoRA layer.

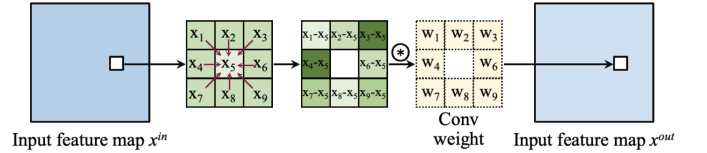


Fig. 4. Illustration of the Central-Difference Convolution (CDC) pipeline.

in practical scenarios. We integrate forgery-aware PEFT modules into plain ViTs. These modules include the LoRA layer, injected into the self-attention blocks, and the adapter layer, integrated into the feed-forward networks (FFN).

As Fig. 3 (c) depicts, the input hidden state h^{in} is simultaneously forwarded to the fixed ImageNet MLP weights and the designed trainable convolutional layers. Subsequently, the outputs of these processes are element-wise summed before being passed to the subsequent vision transformer blocks:

$$h^{out} = \text{MLP}(h^{in}) + \text{Adapter}(h^{in}). \quad (1)$$

The Adapter layer is formulated as:

$$\text{Adapter}(h^{in}) = \text{Conv}_{1 \times 1}^{\text{up}}(\text{CDC}(\text{Conv}_{1 \times 1}^{\text{down}}(h^{in}))). \quad (2)$$

We first expand the input hidden state h^{in} into a 2-D dimension. Next, we reduce the dimension of the expanded feature using a 1×1 convolutional layer, effectively decreasing the number of parameters activated in the Adapter layer. We then design the Central Difference Convolution (CDC) operator to expose local forgery artifacts for each input query. The pipeline of the CDC operator is illustrated in Fig. 4. The output feature map x^{out} can be calculated by:

$$x^{out} = \sum_{i \in \Omega} w_i (x_i^{in} - x_c), \quad (3)$$

where x_c indicates the center pixel of the window Ω , and x_5 represents x_c in Fig. 4. x_i indicates the peripheral pixels within Ω . w_i denotes the corresponding convolutional weights. Finally, the second 1×1 Conv layer restores the channels of the feature, and the produced feature is flattened to the same shape as h^{in} . Our designed adapter layer effectively introduces inductive bias into standard ViTs, guiding the model in learning local artifacts for face forgery detection.

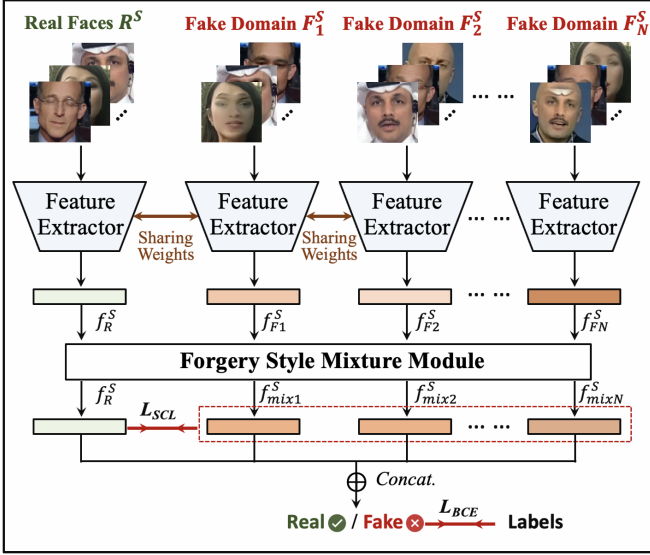


Fig. 5. Illustration of forgery style mixture pipeline. The designed feature extractor processes real faces and forgery source domain data, and the extracted features are subsequently delivered to the forgery-style mixture module.

Additionally, considering the effectiveness of high-frequency features in the task of face forgery detection [6], [36]–[38], our CDC operator enables the model to extract abundant high-frequency information from input faces, thereby enhancing detection performance.

In addition to the Adapter layer, which introduces local dependencies into plain ViT backbones, we further design the Low-Rank Adaptation (LoRA) layer to obtain global receptive fields with minimal parameters. As depicted in Fig. 3 (d), the output hidden state h^{out} is calculated by:

$$h^{out} = W_{q/k/v} h^{in} + \text{LoRA}(h^{in}). \quad (4)$$

The $W_{q/k/v}$ parameter denotes the pre-trained ImageNet weights fixed during the training process. Moreover, the LoRA module consists of two low-rank matrices:

$$\text{LoRA}(h^{in}) = h^{in} W_{q/k/v}^{down} W_{q/k/v}^{up}, \quad (5)$$

where $h^{in} \in \mathbb{R}^{d \times d}$, $W_{q/k/v}^{down} \in \mathbb{R}^{d \times r}$, $W_{q/k/v}^{up} \in \mathbb{R}^{r \times d}$, and $r \ll d$. We optimize the slim, decomposed low-rank matrices during training instead of the redundant pre-trained weights. As such, the number of trainable parameters is significantly reduced. In this work, we set the hidden state dimension d of ViT-B to 768, and the rank r is defaulted to 8.

The designed forgery-aware PEFT modules bear the following advantages for face forgery detection: (1) they effectively preserve knowledge learned from ImageNet, while adaptively learning forgery-specific information; and (2) they simultaneously capture expressive global features and extract informative local forgery clues, thereby enhancing the final detection performance. These advantages jointly contribute to a more generalized approach to face forgery detection.

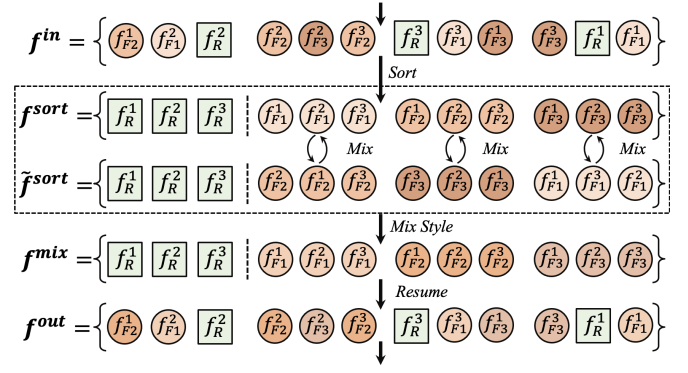


Fig. 6. Pipeline of the proposed forgery feature mixture process.

C. Forgery style mixture

In face forgery detection, the training dataset often encompasses multiple forgery techniques. This training setting accommodates practical scenarios where available source domains are utilized. In this vein, we denote the training dataset as $D^S = \{R^S, F_1^S, F_2^S, \dots, F_N^S\}$. R^S denotes the source real faces, and F_i^S is the i_{th} source forgery domain, $i \in \{1, 2, \dots, N\}$. As such, the testing data can be denoted as $D^T = \{R^T, F_1^T, F_2^T, \dots, F_M^T\}$. Similarly, R^T and F^T are target real and forgery domains, while M denotes the number of target forgery domains. Our preliminary experiment, illustrated in Fig. 1, reveals a high false negative rate (FNR) and a low false positive rate (FPR) in cross-domain evaluations, suggesting a negligible domain gap between R^S and R^T and significant domain gaps between F^S and F^T . As such, we need to augment source forgery domains to mitigate this issue. Fig. 5 depicts the proposed forgery-style mixture pipeline. The training batch $X^S = \{R^S, F_1^S, F_2^S, \dots, F_N^S\}$ is processed by our designed feature extractor, which shares weights across all source domains. The extracted features from the source forgery domains are combined in the designed forgery-style mixture module, and the mixed features are forwarded to the classifier to perform forgery detection.

Next, we elaborate on the details of the devised forgery style mixture module, as depicted in Fig. 6. This module processes a training batch of real and forged face images sampled from N source domains, where $N = 3$, for instance, is shown in Fig. 6. Green squares denote real faces in this representation, while red circles indicate the forgery faces. The input feature f^{in} proceeds to our designed Forgery Style Mixture module.

We first sort f^{in} to f^{sort} according to the domain labels, where f_R represents real features, and f_{F_i} with $i \in \{1, 2, 3\}$, denotes features from distinct forgery domains. The superscript of each sample indicates the feature index of the domain. To augment the forgery style, we first shuffle the fake features of f^{sort} , ensuring that each forgery domain label of the shuffled \tilde{f}^{sort} differs from the original f^{sort} . In addition, we keep the real feature order unchanged. Subsequently, we blend the forgery feature styles of the original f^{sort} and the shuffled \tilde{f}^{sort} .

We draw inspiration from Adaptive Instance Normalization (AdaIN) [39], a widely employed image style transfer tech-

nique. The source style of p can be transferred to the target style of q by:

$$\text{AdaIN}(p) = \sigma(q) \frac{p - \mu(p)}{\sigma(p)} + \mu(q), \quad (6)$$

where $\mu(p)$ and $\sigma(p)$ are the spatial mean and standard deviation of the feature tensor p .

Inspired by the AdaIN, which utilizes the feature statistics of a target style input to transfer the image style, we first calculate the mixed feature statistics of f and \tilde{f} :

$$\gamma_{mix} = \delta\sigma(f) + (1 - \delta)\sigma(\tilde{f}), \quad (7)$$

$$\eta_{mix} = \delta\mu(f) + (1 - \delta)\mu(\tilde{f}), \quad (8)$$

where δ is a weight sampled from Beta distribution, i.e., $\delta \sim \text{Beta}(0.1, 0.1)$. γ_{mix} and η_{mix} are the weighted summation of the forgery style statistics of f and \tilde{f} . Then, the style mixture is performed by the mixed feature statistics γ_{mix} and η_{mix} to the original feature f :

$$f_{mix} = \text{MixStyle}(f) = \gamma_{mix} \frac{f - \mu(f)}{\sigma(f)} + \eta_{mix}. \quad (9)$$

Similar to [40], we set a default probability of 0.5 to activate the forgery-style mixture module. Finally, we restore the original index order of the mixed features f^{sort} to obtain f^{out} , which is forwarded to the classifier for final decision-making. In the inference stage, the forgery-style mixture is deactivated.

During training, the designed forgery-style mixture module augments the source forgery domains, effectively mitigating the overfitting problem and enhance the model's generalizability. This design enhances the model's generalization for open-set face forgery detection.

D. Objective function

During training, as we augment source-forgery features using the designed forgery style mixture module, we must train a classifier that can effectively distinguish between real face features and the augmented forgery features. Therefore, this work adopts the Single-Center Loss (SCL) [45] to obtain a clearer boundary between bonafide and fake faces. The overall objective function consists of two losses:

$$L = L_{BCE} + \lambda L_{SCL}, \quad (10)$$

where λ balances the two loss components. L_{BCE} represents the binary cross-entropy loss. The Single-Center Loss, denoted as L_{SCL} , aims to compact the feature distribution of real faces while simultaneously moving fake features away from the center of real features:

$$L_{SCL} = \text{Dist}_R + \max(\text{Dist}_R - \text{Dist}_F + \text{margin}, 0) \quad (11)$$

where Dist_R and Dist_F denote the average distance between the real feature center C and real feature f_R and fake feature f_F , respectively:

$$\text{Dist}_R = \frac{1}{N_R} \sum_{i=1}^{N_R} \|f_R^i - C\|_2; \quad \text{Dist}_F = \frac{1}{N_F} \sum_{j=1}^{N_F} \|f_F^j - C\|_2 \quad (12)$$

where the real center C is the average of all N_R real features f_R :

$$C = \frac{1}{N_R} \sum_{i=1}^{N_R} f_R^i. \quad (13)$$

We select the features after the second-to-last fully-connected layer to calculate L_{SCL} . This loss enhances the discriminative and separable characteristics of the real and fake face features, thereby improving the overall performance of face forgery detection.

IV. EXPERIMENTS AND RESULTS

A. Experimental setup

1) *Implementation details*: In this study, we employ the popular `dlib` face detector [47] to crop face regions. The proposed framework is implemented on the PyTorch [48] platform, and the model is trained using Adam optimizer [49] with $\beta_1 = 0.9$ and $\beta_2 = 0.999$. We set the learning rate at $3e-5$, and no learning rate decay is applied throughout the whole training process. Our default architecture employs the ViT-B as the backbone, and we train the model on a single 2080Ti GPU with a batch size of 48. The training comprises 30,000 iterations, and the ViT-B parameters are initialized with ImageNet-21k [50] weights.

2) *Datasets*: We adopt the FaceForensics++ (FF++) dataset [51] for training, which includes original real videos (OR) and four types of forgeries: Deepfakes (DF) [52], Face2Face (FF) [53], FaceSwap (FS) [54], and NeuralTextures (NT) [55]. Each category comprises 1,000 videos in raw, high-quality (c23), and low-quality (c40) formats. Following the official data split strategy [51], we allocate 720 videos for training, 140 for validation, and 140 for testing. Raw videos represent non-compressed videos, whereas c23 and c40 videos denote slightly compressed and highly compressed videos. Our experiments exclusively employ the compressed c23 and c40 videos to align with practical applications.

3) *Evaluation Metrics*: To facilitate head-to-head comparisons with previous methodologies, we employ Accuracy (ACC), Area Under the receiver operating characteristic Curve (AUC), and Equal Error Rate (EER) as the evaluation metrics in this work. ACC is a straightforward metric that quantifies the proportion of correctly classified samples from the total number of samples. AUC measures the Area under the Receiver Operating Characteristic (ROC) curve. EER denotes the point of ROC where False Positive Rate (FPR) is equal to the True Positive Rate (TPR). Unless specified otherwise, we report the image-level detection results throughout this paper.

B. Cross-manipulation evaluation

In real-world applications, face forgery detectors inevitably encounter data generated by new forgery techniques, leading to significant performance drops. To evaluate the generalization capability, we train the models on the training sets comprising three source manipulation types of FF++. Subsequently, we evaluate the trained models on the test sets of the unseen target manipulation type. Table I presents the detection AUC and ACC of different models on the FF++ high-quality (c23)

TABLE I
HIGH QUALITY (C23) CROSS-MANIPULATION DETECTION PERFORMANCE ON UNSEEN FORGERY METHODS. THE TRAINABLE PARAMETER NUMBER OF EACH MODEL IS REPORTED TO EVALUATE THE TRAINING EFFICIENCY.

Method	Venue	#Params	FF,FS,NT→DF		DF,FS,NT→FF		DF,FF,NT→FS		DF,FF,FS→NT		Average	
			AUC	ACC								
ResNet18 [41]	CVPR16	11.18M	0.813	0.656	0.746	0.596	0.464	0.476	0.688	0.528	0.678	0.564
Xception [10]	CVPR17	20.81M	0.907	0.795	0.753	0.558	0.460	0.472	0.744	0.557	0.716	0.596
EN-B4 [11]	ICML19	19.34M	0.485	0.495	0.556	0.523	0.517	0.517	0.493	0.500	0.513	0.509
All-train EN-B4 [11]	ICML19	19.34M	0.911	0.824	0.801	0.633	0.543	0.500	0.774	0.608	0.757	0.641
Focal-loss EN-B4 [11]	ICML19	19.34M	0.903	0.813	0.798	0.608	0.503	0.484	0.759	0.604	0.741	0.627
Forensics Transfer [42]	ArXiv18	-	-	0.720	-	0.645	-	0.460	-	0.569	-	0.599
Multi-task [43]	BTAS19	-	-	0.703	-	0.587	-	0.497	-	0.603	-	0.598
MLDG [44]	AAAI18	62.38M	0.918	0.842	0.771	0.634	0.609	0.527	<u>0.780</u>	0.621	0.770	0.656
LTW [45]	AAAI21	20.37M	0.927	0.856	0.802	0.656	0.640	0.549	0.773	<u>0.653</u>	0.786	0.679
ViT-B [16]	ICLR21	85.80M	0.771	0.701	0.656	0.582	0.510	0.498	0.554	0.517	0.623	0.575
CFM [46]	TIFS24	25.37M	0.880	0.617	0.814	0.557	0.631	0.516	0.644	0.508	0.742	0.550
SCLoRA [21]	MIPR23	4.72M	0.935	0.862	0.875	0.753	0.651	0.554	0.707	0.626	0.792	0.699
OSDFD	Ours	1.34M	0.962	0.885	0.932	0.846	0.698	0.595	0.781	0.682	0.843	0.752

TABLE II
LOW QUALITY (C40) CROSS-MANIPULATION DETECTION PERFORMANCE ON UNSEEN FORGERY METHODS. THE TRAINABLE PARAMETER NUMBER OF EACH MODEL IS REPORTED TO EVALUATE THE TRAINING EFFICIENCY.

Method	Venue	#Params	FF,FS,NT→DF		DF,FS,NT→FF		DF,FF,NT→FS		DF,FF,FS→NT		Average	
			AUC	ACC								
ResNet18 [41]	CVPR16	11.18M	0.741	0.673	0.648	0.600	0.634	0.594	0.598	0.567	0.655	0.609
Xception [10]	CVPR17	20.81M	0.766	0.694	0.696	0.643	0.626	0.593	0.597	0.552	0.671	0.621
EN-B4 [11]	ICML19	19.34M	0.451	0.485	0.537	0.505	0.512	0.503	0.499	0.497	0.500	0.498
All-train EN-B4 [11]	ICML19	19.34M	0.753	0.676	0.674	0.614	0.614	0.580	0.600	0.564	0.660	0.609
Focal-loss EN-B4 [11]	ICML19	19.34M	0.749	0.674	0.672	0.610	0.596	0.575	0.605	0.566	0.656	0.606
Forensics Transfer [42]	ArXiv18	-	-	0.682	-	0.550	-	0.530	-	0.550	-	0.578
Multi-task [43]	BTAS19	-	-	0.667	-	0.565	-	0.517	-	0.560	-	0.577
MLDG [44]	AAAI18	62.38M	0.730	0.671	0.617	0.581	0.617	0.581	0.607	0.569	0.643	0.601
LTW [45]	AAAI21	20.37M	0.756	0.691	0.724	0.657	0.681	0.625	<u>0.608</u>	<u>0.585</u>	0.692	0.640
ViT-B [16]	ICLR21	85.80M	0.739	0.643	0.650	0.595	0.592	0.560	<u>0.552</u>	<u>0.538</u>	0.633	0.584
CFM [46]	TIFS24	25.37M	0.789	0.686	0.622	0.541	0.688	0.607	0.566	0.517	0.666	0.588
SCLoRA [21]	MIPR23	4.72M	0.818	0.735	0.686	0.638	0.710	0.653	0.582	0.542	0.699	0.642
OSDFD	Ours	1.34M	0.853	0.762	<u>0.717</u>	0.663	0.713	0.661	0.630	0.595	0.728	0.670

dataset. We bold the best detection results and underline the second-best results. It can be observed that OSDFD achieves SOTA AUC and ACC performances across all experiments.

Moreover, generalization to poor-quality data is crucial for real-world face forgery detectors. Therefore, we conduct the cross-manipulation experiments on low-quality (c40) data, as shown in Table II, where OSDFD outperforms previous approaches by a significant margin. This underscores the proposed method’s outstanding generalizability across diverse data qualities. Additionally, our approach demonstrates substantial improvements over the ViT-B baseline, demonstrating the effectiveness of the designed framework. Furthermore, compared to our conference version SCLoRA [21], our method consistently achieves superior performance on both c23 and c40 data, which can be attributed to the effectiveness of the designed forgery style mixture module and local CDC feature extractor. Finally, OSDFD comprises the fewest 1.34M trainable parameters, facilitating its deployment in real-world applications, particularly on mobile devices.

C. Cross-dataset evaluation

Due to the significant domain gaps between training and testing datasets [59], [60] in face forgery detection, cross-dataset evaluation has been a persistent challenge. We further

conduct cross-dataset evaluations to assess the generalizability of forgery detectors. We train the models on the FF++ (c23) training set (OR, DF, FF, FS, and NT) and test them on six popular Deepfake datasets, including CelebDF-v2 (CDF) [61], WildDeepfake (WDF) [62], DeepFake Detection Challenge (DFDC) [63], DeepFake Detection Challenge Preview (DFDC-P) [63], DeepForensics-1.0 (DFR) [64], and Face Forensics in the Wild (FFIW) [65]. These testing datasets simulate real-world scenarios well, encompassing various environmental variables. AUC and EER performance are reported in Table III, where ‘*’ indicates the trained model provided by the authors, and ‘†’ indicates our re-implementation using the public official code. The upper table presents the frame-level detection results, while the blue-highlighted bottom table shows video-level results. Video-level detection scores are calculated by averaging all frame scores within each video. The best and second-best results are highlighted in bold and underlined, respectively. The trainable parameter number of each detector is provided in the table for reference. Our method, OSDFD, achieves the highest average detection performance in both frame-level and video-level evaluation, with only 1.34M activated parameters. Compared to the ViT-B backbone, OSDFD consistently demonstrates significant performance improvements across all six datasets, demonstrating its exceptional

TABLE III

CROSS-DATASET EVALUATION ON SIX UNSEEN DATASETS. ‘*’ INDICATES THE TRAINED MODEL PROVIDED BY THE AUTHORS. ‘†’ INDICATES OUR RE-IMPLEMENTATION USING THE PUBLIC OFFICIAL CODE. METHODS HIGHLIGHTED IN BLUE DENOTE VIDEO-LEVEL RESULTS. THE TRAINABLE PARAMETER NUMBER OF EACH MODEL IS REPORTED TO EVALUATE THE TRAINING EFFICIENCY.

Method	Venue	#Params	CDF		WDF		DFDC-P		DFDC		DFR		FFIW		Average	
			AUC	EER	AUC	EER	AUC	EER	AUC	EER	AUC	EER	AUC	EER	AUC	EER
Face X-ray [13]	CVPR20	41.97M	74.20	-	-	-	70.00	-	-	-	-	-	-	-	-	-
GFF [24]	CVPR21	53.25M	75.31	32.48	66.51	41.52	71.58	34.77	-	-	-	-	-	-	-	-
LTW [45]	AAAI21	20.37M	77.14	29.34	67.12	39.22	74.58	33.81	-	-	-	-	-	-	-	-
F2Trans-S [28]	TIFS23	117.52M	80.72	-	-	-	71.71	-	-	-	-	-	-	-	-	-
SBI* [14]	CVPR22	19.34M	81.33	26.94	67.22	38.85	79.87	28.26	68.45	37.23	84.90	23.13	81.47	27.33	77.21	30.29
DCL* [15]	AAAI22	19.35M	81.05	26.76	72.95	35.73	71.49	35.90	<u>72.69</u>	34.91	92.26	14.81	82.08	27.75	78.75	29.31
Xception† [10]	ICCV19	20.81M	64.14	39.77	68.90	38.67	69.56	36.94	<u>64.52</u>	39.29	91.93	15.52	77.58	31.21	72.77	33.57
RECCE† [56]	CVPR22	25.83M	61.42	41.71	74.38	32.64	64.08	40.04	67.61	36.98	92.93	14.74	85.84	<u>24.12</u>	74.38	31.71
EN-B4† [11]	ICML19	19.34M	65.24	39.41	67.89	37.21	67.96	37.60	63.48	40.14	92.18	15.51	70.03	35.40	71.13	35.40
CFM [46]	TIFS24	25.37M	<u>82.78</u>	<u>24.74</u>	<u>78.39</u>	<u>30.79</u>	75.82	31.67	68.28	37.14	<u>95.18</u>	11.87	78.71	29.28	<u>79.86</u>	27.58
ViT-B [16]	ICLR21	85.80M	<u>72.35</u>	<u>34.50</u>	<u>75.29</u>	<u>33.40</u>	75.58	32.11	71.48	35.54	<u>80.47</u>	26.97	68.49	37.12	<u>73.94</u>	33.27
SCLoRA [21]	MIPR23	4.72M	73.56	32.87	77.91	29.56	<u>77.08</u>	<u>30.37</u>	72.32	<u>34.52</u>	94.78	11.76	81.42	26.59	79.51	26.59
OSDFD	Ours	1.34M	83.35	24.47	78.53	28.46	76.28	31.17	75.52	31.99	95.54	9.90	<u>84.61</u>	24.09	82.31	25.01
Lisiam [57]	TIFS22	-	78.21	-	-	-	-	-	-	-	-	-	-	-	-	-
F3Net [6]	ECCV20	42.53M	68.69	-	-	-	67.45	-	-	-	-	-	-	-	-	-
FTCN [58]	ICCV21	26.60M	86.90	-	-	-	74.00	-	-	-	-	-	-	-	-	-
SBI* [14]	CVPR22	19.34M	88.61	19.41	70.27	37.63	84.80	25.00	71.70	35.27	90.04	17.53	86.34	23.45	81.96	26.38
DCL* [15]	AAAI22	19.35M	88.24	19.12	76.87	31.44	77.57	29.55	75.03	30.94	97.41	9.96	86.26	24.32	83.56	24.22
RECCE† [56]	CVPR22	25.83M	69.25	34.38	76.99	30.49	66.90	39.39	70.26	34.25	97.15	9.29	92.05	<u>17.74</u>	78.77	27.59
CFM [46]	TIFS24	25.37M	<u>89.65</u>	<u>17.65</u>	<u>82.27</u>	26.80	<u>80.22</u>	27.48	70.59	35.02	97.59	9.04	83.81	24.49	<u>84.02</u>	<u>23.41</u>
ViT-B [16]	ICLR21	85.80M	78.12	30.59	78.95	29.59	79.43	28.62	73.35	33.05	86.42	19.90	70.34	35.45	<u>77.77</u>	29.53
SCLoRA [21]	MIPR23	4.72M	81.11	26.32	82.78	24.85	80.20	26.68	74.96	35.01	98.53	6.63	85.59	22.70	83.86	23.70
OSDFD	Ours	1.34M	90.81	16.94	81.42	24.90	79.49	28.31	78.74	29.37	98.89	4.48	<u>90.01</u>	17.50	86.56	20.25

generalization capability. Furthermore, OSDFD outperforms our conference version SCLoRA by a significant margin, underscoring the effectiveness of the designed CDC Adapter layer and forgery-style mixture module.

D. Robustness evaluation

Videos circulating on social media platforms often undergo various distortions during transmission. To simulate real-world scenarios, we introduce six common perturbations: Gaussian blur, pink noise, white noise, block, brightness, and darkness. Fig. 8 showcases both the original and corresponding distorted face images. We incorporate five severity levels for each perturbation type to mimic unpredictable environments. The robustness evaluation results are depicted in Fig. 7. OSDFD does not employ data augmentations during training, facilitating efficient training, or fine-tuning for real-world applications. All models depicted in Fig. 7 are trained on the FF++ c23 training set, with distortions applied to the corresponding test set. As the severity of distortion increases, all face forgery detection methods experience performance degradation. Compared to previous arts, our proposed approach achieves superior or comparable AUC performance across all six types of perturbation. Furthermore, the average robustness results across all distortions highlight that OSDFD, with the fewest trainable parameters, demonstrates the best robustness against practical image/video perturbations.

E. Ablation study

In this subsection, we carry out extensive ablation experiments to showcase the effectiveness of the designed components, the flexibility of the proposed learning scheme, the rationale behind the adopted training strategy, and the impacts of the mixed features.

TABLE IV
ABLATION EXPERIMENTS ON DIFFERENT MODEL COMPONENTS.
AVERAGE CROSS-MANIPULATION DETECTION PERFORMANCE ON FF++
c23 DATASET.

ViT	LoRA	Adapter	MixStyle	SCL	AUC	ACC
✓	-	-	-	-	0.623	0.575
✓	✓	-	-	-	0.816	0.719
✓	-	✓	-	-	0.825	0.723
✓	✓	✓	-	-	0.832	0.740
✓	✓	✓	✓	-	0.836	0.743
✓	✓	✓	✓	✓	0.843	0.752

1) *Effectiveness of the designed modules:* We conduct ablation experiments to study the impact of each designed module. Table IV reports the average cross-manipulation (c23) detection AUC and ACC scores across four experimental trials. The designed LoRA and Adapter modules significantly enhance the model’s generalizability. The combination of LoRA and Adapter enables the model to simultaneously explore global and local anomalies within input forgery face images, enhancing the final detection performance. The forgery-style mixture module further boosts the AUC and ACC scores by augmenting the forgery source domains during training. The Single-Center Loss (SCL) encourages the real features to cluster more tightly while pushing features from fake images away from the real center. This design leads to a clearer decision boundary between real and fake faces, further enhancing the generalizability of the detection. Overall, the experimental results presented in Table IV underscore the effectiveness of the designed components.

The proposed method showcases its adaptability by being flexibly adapted to other ViT backbones, a practical feature for researchers, engineers, and practitioners in the field of computer vision and image processing. Herein, we assess the face forgery detection performance of our OSDFD on various

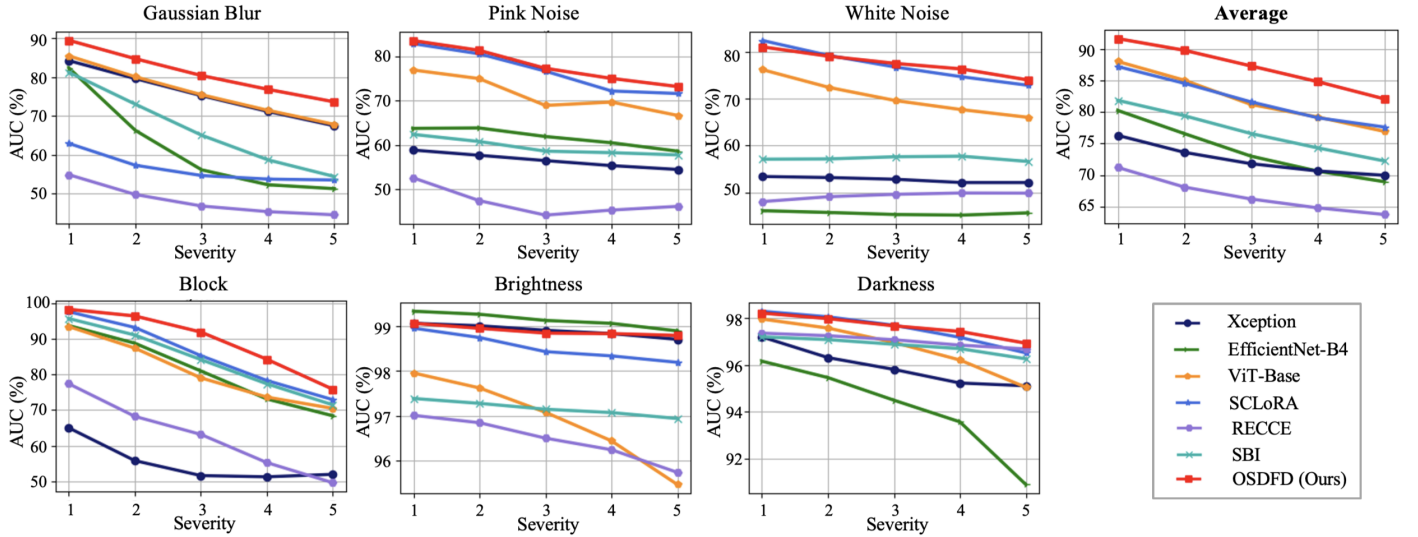


Fig. 7. Robustness to common perturbations at five severity levels: Gaussian Blur, Pink Noise, White Noise, Block, Brightness, and Darkness.

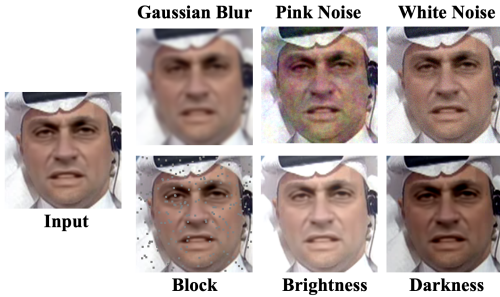


Fig. 8. Input face image and its perturbed versions.

ViT backbones, including ViT-Tiny (ViT-T), ViT-Small (ViT-S), and ViT-Large (ViT-L). The cross-manipulation (c23) AUC results are presented in Table V. It can be readily observed that the average cross-manipulation performance improves with increasing model capacity. Nevertheless, larger ViT models tend to require significantly more computing resources and inference time, thereby impeding their real-world deployment.

In contrast, OSDFD consistently enhances the generalizability of ViT backbones across different model complexities, underscoring its practicality and adaptability. Specifically, our method achieves average AUC enhancements of 11.7%, 15.7%, and 16.7%, respectively. These results demonstrate the capability of OSDFD to seamlessly integrate into existing ViT models in a plug-and-play manner.

In this work, we adopt a Parameter-Efficient Fine-Tuning (PEFT) strategy, a reliable approach, to train the face forgery detection model. Specifically, we only optimize the Adapter and LoRA layers while keeping the other ViT parameters fixed with ImageNet weights. We compare the PEFT strategy with the full fine-tuning (FT) strategy to validate its effectiveness. Table VI presents the cross-manipulation (c23) AUC results, where DF, FF, FS, and NT denote the testing manipulation types. The models are trained on three manipulations and tested on the remaining one. The two experimental settings

TABLE V
CROSS-MANIPULATION AUC PERFORMANCE ON FF++ (C23) DATASET WITH DIFFERENT ViT BACKBONES.

Backbone	OSDFD	DF	FF	FS	NT	AVG
ViT-T	-	0.853	0.658	0.488	0.584	0.646
ViT-T	✓	0.919	0.860	0.563	0.709	0.763
ViT-S	-	0.870	0.688	0.465	0.566	0.647
ViT-S	✓	0.929	0.897	0.600	0.791	0.804
ViT-L	-	0.850	0.708	0.572	0.593	0.681
ViT-L	✓	0.955	0.941	0.710	0.785	0.848

TABLE VI
CROSS-MANIPULATION AUC PERFORMANCE ON FF++ (C23) DATASET WITH DIFFERENT TRAINING STRATEGIES.

Strategy	DF	FF	FS	NT	AVG
Fully FT	0.896	0.731	0.496	0.603	0.682
PEFT (Ours)	0.962	0.932	0.698	0.781	0.843

employ two training strategies while maintaining the same network architectures. The results in Table VI demonstrate that the PEFT approach outperforms the fully FT strategy across all experimental trials. Notably, the average AUC score of PEFT exhibits a substantial enhancement, increasing from 68.2% to 84.3%. Hence, it can be concluded that the improvements in face forgery detection performance benefit from the PEFT strategy adopted. Furthermore, the PEFT strategy effectively preserves the abundant ImageNet prior knowledge while learning the forgery-aware knowledge through the designed Adapter and LoRA modules in an adaptive manner, reinforcing the reliability of our research.

2) *Impacts of different ratios of mixed features*: Our proposed method utilizes a feature mixture module to augment forgery domains in the feature space. As illustrated in Fig. 9, the x -axis represents the ratio of the mixed forgery features among all forgery features. We analyze the impact of this ratio by plotting the cross-manipulation (c23) ACC scores against ratio values in Fig. 9. Similarly, we present the average score

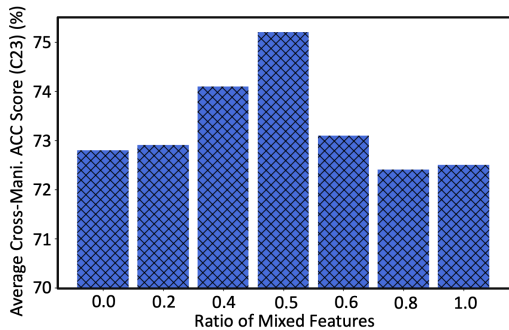


Fig. 9. Average cross-manipulation ACC scores across four experimental trials with respect to different mixed feature ratios.

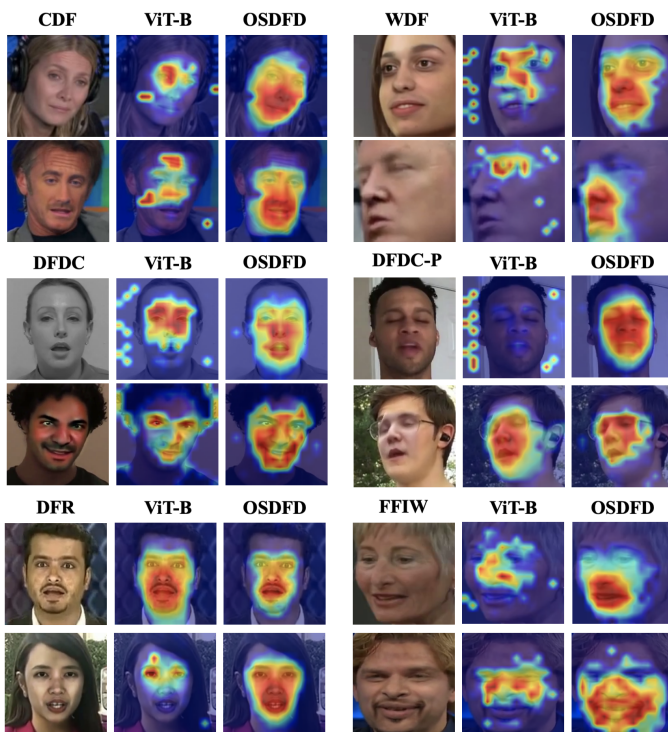


Fig. 10. Grad-CAM [66] visualization results of the ViT-B baseline and OSDFD on six unforescen Deepfake datasets.

across four cross-manipulation evaluation trials. A ratio of ‘0.0’ indicates the pure use of mixed forgery features during training, while ‘1.0’ means no forgery-style mixture is applied. Notably, relying solely on original or mixed forgery features results in limited face forgery detection accuracy. In contrast, combining original and mixed forgery features enhances the model’s generalization capability by augmenting the source forgery domains. The model achieves the highest average ACC score when the ratio of mixed forgery features is 50%. This observation underscores the effectiveness of the designed forgery feature mixture module from another perspective.

F. Visualization results

In this subsection, we provide visualization results to illustrate further the effectiveness of the proposed face forgery detection method.

1) *t-SNE feature map visualization*: In Fig. 11, we present the t-SNE [67] feature embedding visualization results of both the ViT-B baseline and our method OSDFD. Fig. 11 (a) and (b) showcase the results on the unseen CDF dataset, while Fig. 11 (c)-(h) depict the results on the WDF, DFDC, and FFIW datasets, respectively. Red and blue dots represent real and fake data samples in these visualizations. The manifolds of real and fake feature distributions entangle for the baseline model. This observation indicates that the baseline model struggles to discriminate forgery faces from the real ones. In contrast, OSDFD effectively separates real and fake images in the feature space. This improvement underscores the enhanced generalizability achieved by our model, attributed to the designed forgery-style mixture module and forgery-aware PEFT modules.

2) *Grad-CAM map visualization*: We visualize the Grad-CAM [66] maps to identify attention regions of the developed face forgery detector for input queries, as shown in Fig. 10. These maps illustrate the results of the ViT-B baseline model and OSDFD across six unforescen Deepfake datasets: CDF, WDF, DFDC, DFDC-P, DFR, and FFIW. These datasets encompass practical environmental scenarios, including lighting conditions, head poses, image quality, and facial occlusion. Compared to the baseline model, our proposed method accurately highlights informative manipulated regions. The baseline model sometimes focuses on irrelevant non-forgery areas, and these ‘non-interesting’ regions can lead to wrong decisions. Conversely, our method effectively identifies regions with significant forgery artifacts, contributing to superior face forgery detection performance. Specifically, our approach consistently demonstrates outstanding gradient-based localization across diverse environmental variables, such as extreme head poses in WDF, abnormal color hues in DFDC, facial occlusion (glasses) in DFDC-P, and extreme facial area ratios in FFIW. These observations further underscore the outstanding generalizability of our method in real-world applications.

V. CONCLUSIONS AND FUTURE WORK

This paper introduces a parameter-efficient and generalized approach towards open-set face forgery detection. Our method, OSDFD, incorporates lightweight LoRA and Adapter layers into ViT backbones, updating only these modules during training to learn global and local forgery-aware features efficiently. On the other hand, we propose a novel forgery-style mixture module that augments the forgery source domains. In this vein, our method achieves SOTA generalizability and robustness in face forgery detection. An ablation study further underscores that the designed network modules and objective functions contribute to the final detection performance. Our proposed method, OSDFD, can be flexibly adapted to other backbones in a plug-and-play manner. Further ablation experiments demonstrate that the adopted parameter-efficient training strategy is effective in face forgery detection. Our proposed method will shed light on developing future face forgery detectors for real-world applications.

While our proposed method is effective, we limit our scope herein to non-sequential Deepfake detection. Adapting our

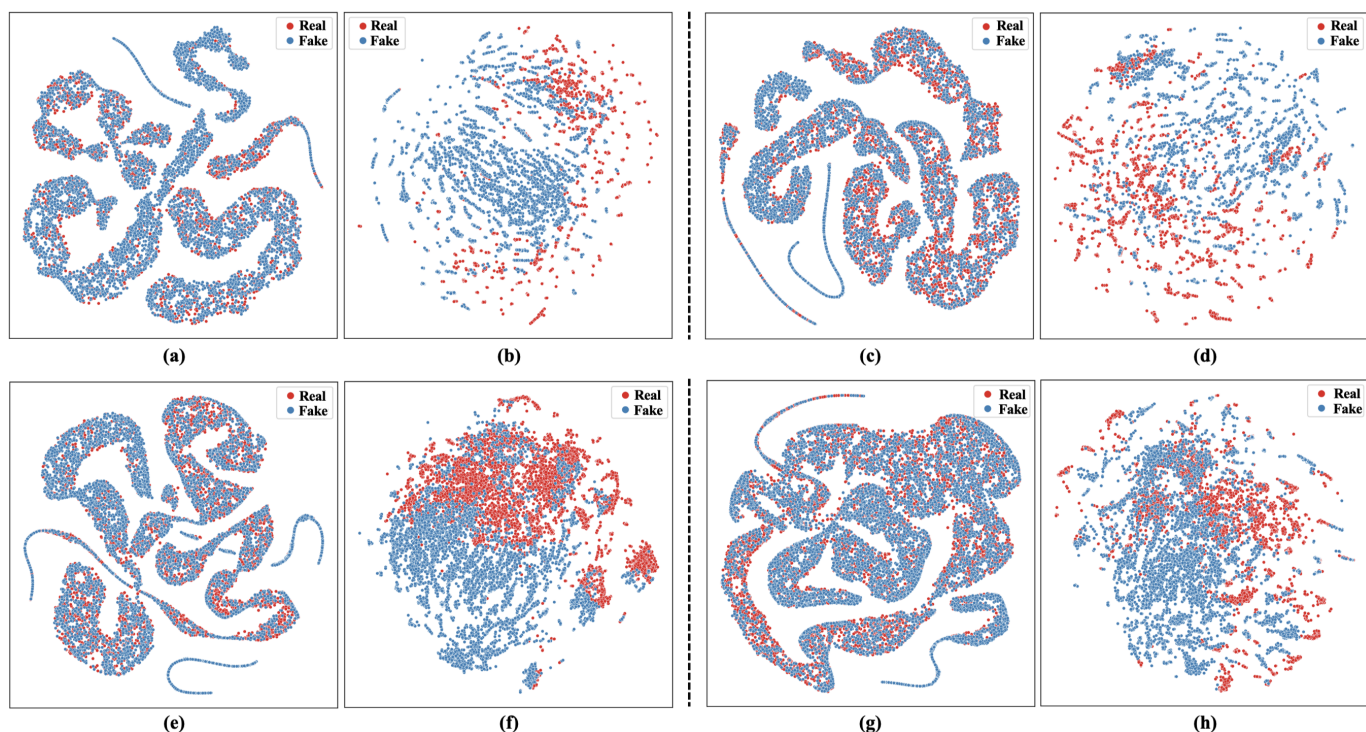


Fig. 11. t-SNE feature embedding visualization of (a) the ViT-B baseline on the CDF dataset, (b) OSDFD on the CDF dataset, (c) the ViT-B baseline on the WDF dataset, (d) OSDFD on the WDF dataset, (e) the ViT-B baseline on the DFDC dataset, (f) OSDFD on the DFDC dataset, (g) the ViT-B baseline on the FFIW dataset, and (h) OSDFD on the FFIW dataset. The red and blue dots represent real and fake data samples, respectively.

approach to leverage abundant sequential information could significantly improve video-level face forgery detection. The designed components can be seamlessly integrated into video transformers, achieving superior performance in uncontrolled environments. This path can be explored in future work.

REFERENCES

- [1] C. Kong, S. Wang, and H. Li, "Digital and physical face attacks: Reviewing and one step further," *arXiv preprint arXiv:2209.14692*, 2022.
- [2] J. P. Cardenuto, J. Yang, R. Padilha, R. Wan, D. Moreira, H. Li, S. Wang, F. Andaló, S. Marcel, A. Rocha *et al.*, "The age of synthetic realities: Challenges and opportunities," *APSIPA Transactions on Signal and Information Processing*, vol. 12, no. 1, 2023.
- [3] S. M. Daniel Moreira and A. Rocha, "Synthetic realities and artificial intelligence-generated contents," *IEEE Security & Privacy*, vol. 22, no. 3, pp. 7–10, 2024.
- [4] X. Wang, T. Yao, S. Ding, and L. Ma, "Face manipulation detection via auxiliary supervision," in *International Conference on Neural Information Processing*. Springer, 2020, pp. 313–324.
- [5] H. Li, B. Li, S. Tan, and J. Huang, "Identification of deep network generated images using disparities in color components," *Signal Processing*, vol. 174, p. 107616, 2020.
- [6] Y. Qian, G. Yin, L. Sheng, Z. Chen, and J. Shao, "Thinking in frequency: Face forgery detection by mining frequency-aware clues," in *European Conference on Computer Vision*. Springer, 2020, pp. 86–103.
- [7] Y. Li, M.-C. Chang, and S. Lyu, "In icu oculi: Exposing ai created fake videos by detecting eye blinking," in *2018 IEEE International Workshop on Information Forensics and Security (WIFS)*. IEEE, 2018, pp. 1–7.
- [8] X. Yang, Y. Li, and S. Lyu, "Exposing deep fakes using inconsistent head poses," in *ICASSP 2019-2019 IEEE International Conference on Acoustics, Speech and Signal Processing (ICASSP)*. IEEE, 2019, pp. 8261–8265.
- [9] Y. Li and S. Lyu, "Exposing deepfake videos by detecting face warping artifacts," *arXiv preprint arXiv:1811.00656*, 2018.
- [10] F. Chollet, "Xception: Deep learning with depthwise separable convolutions," in *Proceedings of the IEEE conference on computer vision and pattern recognition*, 2017, pp. 1251–1258.
- [11] M. Tan and Q. Le, "Efficientnet: Rethinking model scaling for convolutional neural networks," in *International Conference on Machine Learning*. PMLR, 2019, pp. 6105–6114.
- [12] H. H. Nguyen, J. Yamagishi, and I. Echizen, "Capsule-forensics: Using capsule networks to detect forged images and videos," in *ICASSP 2019-2019 IEEE International Conference on Acoustics, Speech and Signal Processing (ICASSP)*. IEEE, 2019, pp. 2307–2311.
- [13] L. Li, J. Bao, T. Zhang, H. Yang, D. Chen, F. Wen, and B. Guo, "Face x-ray for more general face forgery detection," in *Proceedings of the IEEE/CVF conference on computer vision and pattern recognition*, 2020, pp. 5001–5010.
- [14] K. Shiohara and T. Yamasaki, "Detecting deepfakes with self-blended images," in *Proceedings of the IEEE/CVF Conference on Computer Vision and Pattern Recognition*, 2022, pp. 18 720–18 729.
- [15] K. Sun, T. Yao, S. Chen, S. Ding, J. Li, and R. Ji, "Dual contrastive learning for general face forgery detection," in *Proceedings of the AAAI Conference on Artificial Intelligence*, vol. 36, no. 2, 2022, pp. 2316–2324.
- [16] A. Dosovitskiy, L. Beyer, A. Kolesnikov, D. Weissenborn, X. Zhai, T. Unterthiner, M. Dehghani, M. Minderer, G. Heigold, S. Gelly *et al.*, "An image is worth 16x16 words: Transformers for image recognition at scale," *arXiv preprint arXiv:2010.11929*, 2020.
- [17] X. Dong, J. Bao, D. Chen, T. Zhang, W. Zhang, N. Yu, D. Chen, F. Wen, and B. Guo, "Protecting celebrities from deepfake with identity consistency transformer," in *Proceedings of the IEEE/CVF Conference on Computer Vision and Pattern Recognition*, 2022, pp. 9468–9478.
- [18] R. Shao, T. Wu, and Z. Liu, "Detecting and recovering sequential deepfake manipulation," in *European Conference on Computer Vision*. Springer, 2022, pp. 712–728.
- [19] W. Zhuang, Q. Chu, Z. Tan, Q. Liu, H. Yuan, C. Miao, Z. Luo, and N. Yu, "Uia-vit: Unsupervised inconsistency-aware method based on vision transformer for face forgery detection," in *European Conference on Computer Vision*. Springer, 2022, pp. 391–407.
- [20] Y. Yu, R. Ni, S. Yang, Y. Zhao, and A. C. Kot, "Narrowing domain gaps with bridging samples for generalized face forgery detection," *IEEE Transactions on Multimedia*, vol. 26, pp. 3405–3417, 2024.
- [21] C. Kong, H. Li, and S. Wang, "Enhancing general face forgery detection via vision transformer with low-rank adaptation," *IEEE 6th Interna-*

- tional Conference on Multimedia Information Processing and Retrieval (MIPR), 2023.
- [22] U. A. Ciftci, I. Demir, and L. Yin, "Fakecatcher: Detection of synthetic portrait videos using biological signals," *IEEE transactions on pattern analysis and machine intelligence*, 2020.
- [23] C. Kong, B. Chen, H. Li, S. Wang, A. Rocha, and S. Kwong, "Detect and locate: Exposing face manipulation by semantic-and noise-level telltales," *IEEE Transactions on Information Forensics and Security*, vol. 17, pp. 1741–1756, 2022.
- [24] Y. Luo, Y. Zhang, J. Yan, and W. Liu, "Generalizing face forgery detection with high-frequency features," in *Proceedings of the IEEE/CVF Conference on Computer Vision and Pattern Recognition*, 2021, pp. 16 317–16 326.
- [25] A. Luo, C. Kong, J. Huang, Y. Hu, X. Kang, and A. C. Kot, "Beyond the prior forgery knowledge: Mining critical clues for general face forgery detection," *IEEE Transactions on Information Forensics and Security*, vol. 19, pp. 1168–1182, 2023.
- [26] J. Wang, Z. Wu, W. Ouyang, X. Han, J. Chen, Y.-G. Jiang, and S.-N. Li, "M2tr: Multi-modal multi-scale transformers for deepfake detection," in *Proceedings of the 2022 international conference on multimedia retrieval*, 2022, pp. 615–623.
- [27] J. Guan, H. Zhou, Z. Hong, E. Ding, J. Wang, C. Quan, and Y. Zhao, "Delving into sequential patches for deepfake detection," *Advances in Neural Information Processing Systems*, vol. 35, pp. 4517–4530, 2022.
- [28] C. Miao, Z. Tan, Q. Chu, H. Liu, H. Hu, and N. Yu, "F2trans: High-frequency fine-grained transformer for face forgery detection," *IEEE Transactions on Information Forensics and Security*, vol. 18, pp. 1039–1051, 2023.
- [29] N. Houlsby, A. Giurgiu, S. Jastrzebski, B. Morrone, Q. De Laroussilhe, A. Gesmundo, M. Attariyan, and S. Gelly, "Parameter-efficient transfer learning for nlp," in *International Conference on Machine Learning*. PMLR, 2019, pp. 2790–2799.
- [30] Y.-L. Sung, J. Cho, and M. Bansal, "Lst: Ladder side-tuning for parameter and memory efficient transfer learning," *Advances in Neural Information Processing Systems*, vol. 35, pp. 12 991–13 005, 2022.
- [31] E. J. Hu, Y. Shen, P. Wallis, Z. Allen-Zhu, Y. Li, S. Wang, L. Wang, and W. Chen, "Lora: Low-rank adaptation of large language models," *arXiv preprint arXiv:2106.09685*, 2021.
- [32] M. Jia, L. Tang, B.-C. Chen, C. Cardie, S. Belongie, B. Hariharan, and S.-N. Lim, "Visual prompt tuning," in *European Conference on Computer Vision*. Springer, 2022, pp. 709–727.
- [33] S. Jie and Z.-H. Deng, "Convolutional bypasses are better vision transformer adapters," *arXiv preprint arXiv:2207.07039*, 2022.
- [34] Y. Zhang, K. Zhou, and Z. Liu, "Neural prompt search," *arXiv preprint arXiv:2206.04673*, 2022.
- [35] V. V. Ramasesh, A. Lewkowycz, and E. Dyer, "Effect of scale on catastrophic forgetting in neural networks," in *International Conference on Learning Representations*, 2021.
- [36] C. Miao, Z. Tan, Q. Chu, N. Yu, and G. Guo, "Hierarchical frequency-assisted interactive networks for face manipulation detection," *IEEE Transactions on Information Forensics and Security*, vol. 17, pp. 3008–3021, 2022.
- [37] J. Fei, Y. Dai, P. Yu, T. Shen, Z. Xia, and J. Weng, "Learning second order local anomaly for general face forgery detection," in *Proceedings of the IEEE/CVF Conference on Computer Vision and Pattern Recognition*, 2022, pp. 20 270–20 280.
- [38] J. Yang, A. Li, S. Xiao, W. Lu, and X. Gao, "Mtd-net: learning to detect deepfakes images by multi-scale texture difference," *IEEE Transactions on Information Forensics and Security*, vol. 16, pp. 4234–4245, 2021.
- [39] X. Huang and S. Belongie, "Arbitrary style transfer in real-time with adaptive instance normalization," in *Proceedings of the IEEE international conference on computer vision*, 2017, pp. 1501–1510.
- [40] K. Zhou, Y. Yang, Y. Qiao, and T. Xiang, "Domain generalization with mixstyle," *arXiv preprint arXiv:2104.02008*, 2021.
- [41] K. He, X. Zhang, S. Ren, and J. Sun, "Deep residual learning for image recognition," in *Proceedings of the IEEE conference on computer vision and pattern recognition*, 2016, pp. 770–778.
- [42] D. Cozzolino, J. Thies, A. Rössler, C. Riess, M. Nießner, and L. Verdoliva, "Forensicttransfer: Weakly-supervised domain adaptation for forgery detection," *arXiv preprint arXiv:1812.02510*, 2018.
- [43] H. H. Nguyen, F. Fang, J. Yamagishi, and I. Echizen, "Multi-task learning for detecting and segmenting manipulated facial images and videos," in *2019 IEEE 10th International Conference on Biometrics Theory, Applications and Systems (BTAS)*. IEEE, 2019, pp. 1–8.
- [44] D. Li, Y. Yang, Y.-Z. Song, and T. Hospedales, "Learning to generalize: Meta-learning for domain generalization," in *Proceedings of the AAAI conference on artificial intelligence*, vol. 32, no. 1, 2018.
- [45] K. Sun, H. Liu, Q. Ye, Y. Gao, J. Liu, L. Shao, and R. Ji, "Domain general face forgery detection by learning to weight," in *Proceedings of the AAAI conference on Artificial Intelligence*, vol. 35, no. 3, 2021, pp. 2638–2646.
- [46] A. Luo, C. Kong, J. Huang, Y. Hu, X. Kang, and A. C. Kot, "Beyond the prior forgery knowledge: Mining critical clues for general face forgery detection," *IEEE Transactions on Information Forensics and Security*, vol. 19, pp. 1168–1182, 2024.
- [47] D. E. King, "Dlib-ml: A machine learning toolkit," *The Journal of Machine Learning Research*, vol. 10, pp. 1755–1758, 2009.
- [48] A. Paszke, S. Gross, F. Massa, A. Lerer, J. Bradbury, G. Chanan, T. Killeen, Z. Lin, N. Gimelshein, L. Antiga et al., "Pytorch: An imperative style, high-performance deep learning library," *Advances in neural information processing systems*, vol. 32, 2019.
- [49] D. P. Kingma and J. Ba, "Adam: A method for stochastic optimization," *arXiv preprint arXiv:1412.6980*, 2014.
- [50] J. Deng, W. Dong, R. Socher, L.-J. Li, K. Li, and L. Fei-Fei, "Imagenet: A large-scale hierarchical image database," in *2009 IEEE conference on computer vision and pattern recognition*. Ieee, 2009, pp. 248–255.
- [51] A. Rossler, D. Cozzolino, L. Verdoliva, C. Riess, J. Thies, and M. Nießner, "Faceforensics++: Learning to detect manipulated facial images," in *Proceedings of the IEEE/CVF International Conference on Computer Vision*, 2019, pp. 1–11.
- [52] "Github deepfake faceswap," <https://github.com/deepfakes/faceswap>, 2018.
- [53] J. Thies, M. Zollhofer, M. Stamminger, C. Theobalt, and M. Nießner, "Face2face: Real-time face capture and reenactment of rgb videos," in *Proceedings of the IEEE conference on computer vision and pattern recognition*, 2016, pp. 2387–2395.
- [54] "Deepfakes faceswap," [EB/OL], 2019, <https://github.com/deepfakes/faceswap>.
- [55] J. Thies, M. Zollhöfer, and M. Nießner, "Deferred neural rendering: Image synthesis using neural textures," *Acm Transactions on Graphics (TOG)*, vol. 38, no. 4, pp. 1–12, 2019.
- [56] J. Cao, C. Ma, T. Yao, S. Chen, S. Ding, and X. Yang, "End-to-end reconstruction-classification learning for face forgery detection," in *Proceedings of the IEEE/CVF Conference on Computer Vision and Pattern Recognition*, 2022, pp. 4113–4122.
- [57] J. Wang, Y. Sun, and J. Tang, "Lisiam: Localization invariance siamese network for deepfake detection," *IEEE Transactions on Information Forensics and Security*, vol. 17, pp. 2425–2436, 2022.
- [58] Y. Zheng, J. Bao, D. Chen, M. Zeng, and F. Wen, "Exploring temporal coherence for more general video face forgery detection," in *Proceedings of the IEEE/CVF international conference on computer vision*, 2021, pp. 15 044–15 054.
- [59] Y. Yu, X. Zhao, R. Ni, S. Yang, Y. Zhao, and A. C. Kot, "Augmented multi-scale spatiotemporal inconsistency magnifier for generalized deepfake detection," *IEEE Transactions on Multimedia*, pp. 1–13, 2023.
- [60] Y. Yu, R. Ni, Y. Zhao, S. Yang, F. Xia, N. Jiang, and G. Zhao, "Msvt: Multiple spatiotemporal views transformer for deepfake video detection," *IEEE Transactions on Circuits and Systems for Video Technology*, vol. 33, no. 9, pp. 4462–4471, 2023.
- [61] Y. Li, X. Yang, P. Sun, H. Qi, and S. Lyu, "Celeb-df: A large-scale challenging dataset for deepfake forensics," in *Proceedings of the IEEE/CVF Conference on Computer Vision and Pattern Recognition*, 2020, pp. 3207–3216.
- [62] B. Zi, M. Chang, J. Chen, X. Ma, and Y.-G. Jiang, "Wildeepfake: A challenging real-world dataset for deepfake detection," in *Proceedings of the 28th ACM International Conference on Multimedia*, 2020, pp. 2382–2390.
- [63] B. Dolhansky, R. Howes, B. Pflaum, N. Baram, and C. C. Ferrer, "The deepfake detection challenge (dfdc) preview dataset," *arXiv preprint arXiv:1910.08854*, 2019.
- [64] L. Jiang, R. Li, W. Wu, C. Qian, and C. C. Loy, "Deepforensics-1.0: A large-scale dataset for real-world face forgery detection," in *Proceedings of the IEEE/CVF Conference on Computer Vision and Pattern Recognition*, 2020, pp. 2889–2898.
- [65] T. Zhou, W. Wang, Z. Liang, and J. Shen, "Face forensics in the wild," in *Proceedings of the IEEE/CVF Conference on Computer Vision and Pattern Recognition (CVPR)*, June 2021, pp. 5778–5788.
- [66] R. R. Selvaraju, M. Cogswell, A. Das, R. Vedantam, D. Parikh, and D. Batra, "Grad-cam: Visual explanations from deep networks via gradient-based localization," in *Proceedings of the IEEE International Conference on Computer Vision*, 2017, pp. 618–626.
- [67] L. Van der Maaten and G. Hinton, "Visualizing data using t-sne." *Journal of machine learning research*, vol. 9, no. 11, 2008.